Improving the Starting Performance of Large Salient-Pole Synchronous Machines

Haran Karmaker, *Senior Member, IEEE,* and Chunting Mi, *Senior Member, IEEE*

***Abstract*—We have carried out an engineering study with the aim of enhancing the reliability of the starting system of the salient-pole synchronous machines in a pumping-generating plant. We focused on accurate prediction of the damper bar currents, electromagnetic torque, acceleration time, and bar temperatures during the starting process. We used the time-stepping finite-element analysis (FEA) for a multiple-pole model including coupled field-circuit formulation and rotor motion. We also developed an analytical model, incorporating the equivalent circuit parameters, to simulate the starting performance of the generator/motor units. The predicted results from both the FEA model and the analytical model agree well with experimental investigations. As a result, we were able to propose a way to improve the motor's reliability and allow many additional starts.**

***Index Terms*—AC generators, equivalent circuits, finite-element analysis (FEA), salient-pole synchronous machines, starting performance, synchronous machines, synchronous motors, time-stepping FEA.**

I. Introduction

PUMP-STORAGE generator/motor units operate economically by generating during periods of peak demand and pumping water to storage reservoirs during off-peak periods. Eight generator/motor units manufactured by the General Electric Company were installed in a pumping/generating plant in the mid-1960s. After over 40 years of reliable operation of the plant, the need for maintenance of the damper winding has increased. The customer requested an engineering study to enhance the reliability of the starting systems of the units to achieve reliable operation of the units. The goal of the engineering study was to identify solutions that would allow the customer to obtain reliable performance of the plant by achieving an additional number of starts in excess of 3000 without any need for major maintenance. The ratings of the 48-pole generator/motor units are shown in Table I. The engineering study is composed of the following major components.

- Review the original design and the expected performance of the damper windings.
- Perform tests to determine the temperature of the damper bars on one of the units. The tests include temperature measurement on all damper bars of a rotor pole during acceleration for both watered and unwatered conditions. Record the acceleration times to reach synchronous speed for both conditions.
- Simulate the starting performance of the machine using equivalent circuit method.
- Generate electromagnetic and thermal finite-element analysis (FEA) models to simulate the test conditions to verify the accuracy of the simulations.
- Conceive and study alternatives to improve the reliability of the starting of the units by using electromagnetic and thermal finite-element simulations.
- Based on the analyses of the alternatives, propose a solution that will allow for the performance of the additional 3000 starts without major maintenance.

TABLE I
RATINGS OF THE STUDIED GENERATOR/MOTOR UNITS

	Power	Power Factor	Speed (RPM)	Voltage (KV)
Generating	53000 KVA	1.0	150	13.8
Motoring	47000 KW	0.95	150	13.2

Due to the advent of powerful computing workstations, the transient analysis of synchronous machines has now become feasible for performing simulation studies using time-stepping FEA including actual stator and rotor winding topology and kinematic equation of rotor motion.

Although the simulation of three-phase sudden short circuit tests by time-stepping finite-element method to derive transient and subtransient reactances during the design of large salient-pole synchronous machines has been reported in the literature [1]–[3], the starting performance calculation of large synchronous machines with fractional-slot stator windings has not been reported.

In [4], the eddy currents in damper bars during starting were calculated for a single-pole finite-element model. It did not include any simulation of kinematic equation of rotor motion. An equivalent circuit approach was presented in [5] using reluctance network in which saturation of magnetic material was included by approximate models of the magnetization characteristics.

The measurement of the torque of large synchronous machines is cumbersome and time consuming [6]. When pulsating torque is included, the task of performing torque measurement is even more difficult [7].

This paper presents the study of the starting performance of the large salient-pole synchronous machine of the pumping-generating plant. An analytical model, based on

Manuscript received February 10, 2004; revised April 16, 2004. This work was supported in part by the Department of Water Resources, California.

H. Karmaker is with General Electric Canada, Peterborough, ON K9J 7B5, Canada (e-mail: haran.karmaker@ps.ge.com).

C. Mi is with the Department of Electrical and Computer Engineering, University of Michigan, Dearborn, MI 48128 USA (e-mail: chrismi@umich.edu).

Digital Object Identifier 10.1109/TMAG.2004.831003

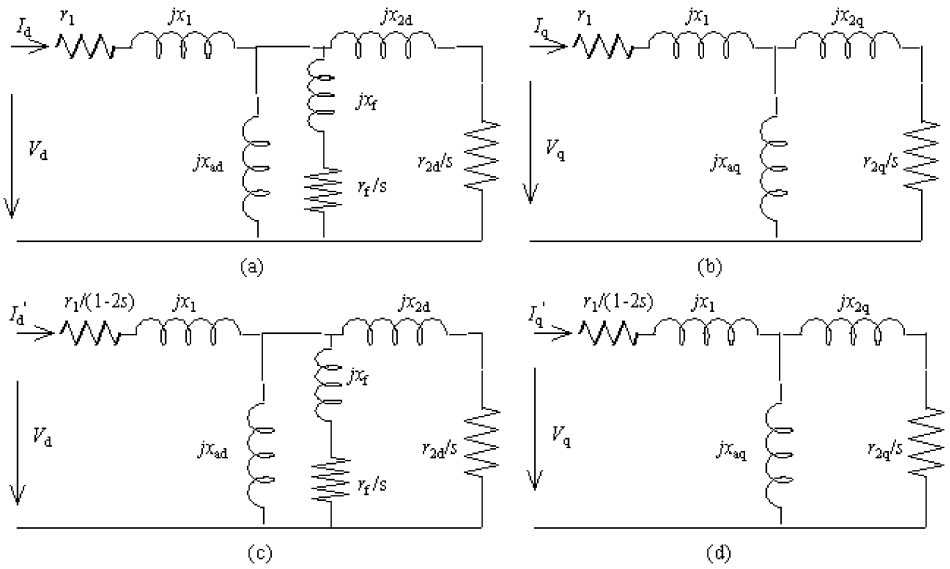

Fig. 1. Equivalent circuit of a synchronous motor during starting. (a) d-axis equivalent circuit for the synchronous components. (b) q-axis equivalent circuit for the synchronous components. (c) d-axis equivalent circuit for the $(1-2s)$ components. (d) q-axis equivalent circuit for the $(1-2s)$ components. The resistance r_f may include a discharge resistance in the field winding. The field is not applied until the speed of the motor reaches about synchronous speed.

equivalent circuit parameters, was developed to simulate the starting performance. Time-stepping FEA, incorporating actual stator and rotor winding topology and kinematic equation of rotor motion, were used for in-depth analysis of the starting performance of the pump-storage motor. All simulation results were confirmed by the on-site measurements. A feasible solution was proposed to extend the additional starts based on these studies.

II. Equivalent Circuit Modeling of the Starting Performance

A. Starting Process

During the starting of salient-pole synchronous motors, the three-phase symmetrical stator currents generate a magnetic field in the air gap, which rotates at synchronous speed ω_1. The synchronous field will induce currents in the rotor damper cages at frequency $s\omega_1$. Due to asymmetry of the rotor, these rotor currents will generate a field which can be decomposed to a positive sequence field and a negative sequence field. The positive sequence field will rotate at speed $s\omega_1$ relative to the rotor. Since rotor rotates at speed ω, this positive field will have the absolute speed equal to synchronous speed $\omega + s\omega_1 = \omega_1$. The negative sequence field generated by the rotor currents will rotate at speed $-s\omega_1$ relative to the rotor. Therefore, the absolute speed of this field is $\omega - s\omega_1 = (1-2s)\omega_1$. This negative sequence field will generate a back-electromotive force (emf) and currents in the stator windings and in the rotor damper cages. The stator currents induced by this field generate a field at the speed of $(1-2s)\omega_1$. The rotor currents induced by this field will have frequency of $-s\omega_1$, which, in turn, will generate a positive sequence field at the speed of $-s\omega_1 + (1-s)\omega_1 = (1-2s)\omega_1$ and a negative sequence field at the speed of $+s\omega_1 + (1-s)\omega_1 = \omega_1$.

The stator and rotor magnetic fields which rotate at the same speed will generate average torque while the fields rotating at different speeds will generate pulsating torque.

B. Equivalent Circuit

The principle of induction motors can be used to derive the equivalent circuit of synchronous machines. Due to the asymmetry of the rotor configuration, the equivalent circuit can be expressed as a d circuit and a q circuit as shown in Fig. 1(a) and (b) for the synchronous components, where all quantities are transferred to the synchronous frame. Since the $(1-2s)\omega_1$ component of stator currents is a negative sequence, all quantities rotate at the speed of $(1-2s)\omega_1$. When transferred to the stator frame (ω_1), the rotor quantities will remain the same as it is in an induction motor but the stator resistance has to be divided by $(1-2s)$, similar to the transformation of the rotor slip of induction machines as shown in Fig. 1(c) and (d).

The significance of Fig. 1 is that all quantities are transferred to the synchronous frame, but each different component sees a different stator resistance. Since all quantities rotate at synchronous speed, the developed torque can be calculated by dividing the power by the synchronous speed.

C. The Developed Torque During Starting

The following assumptions are made for the analysis of the starting performance of large salient-pole synchronous motors. 1) Neglect the saturation. Further, the saturation may be represented by different parameters at different slips. 2) Iron losses, friction loss and windage loss can be considered as part of the developed torque. 3) The motion during starting process is slow such that the slip at each point of the starting process is a constant; and that the cross flux linkage between the d and q axis can be neglected.

Based on the above analysis, assuming a symmetrical power supply, the stator voltage and current during starting can be expressed in the 120 system as

$$V_{120} = \begin{bmatrix} \boldsymbol{V}_1 \\ \boldsymbol{V}_2 \\ \boldsymbol{V}_0 \end{bmatrix} = \begin{bmatrix} V_S e^{j\omega_1 t} \\ V_S e^{-j\omega_1 t} \\ 0 \end{bmatrix} \tag{1}$$

$$I_{120} = \begin{bmatrix} \boldsymbol{I}_1 \\ \boldsymbol{I}_2 \\ \boldsymbol{I}_0 \end{bmatrix} = \begin{bmatrix} \boldsymbol{I}_S + \boldsymbol{I}'_S \\ \boldsymbol{I}^*_S + \boldsymbol{I}'^*_S \\ 0 \end{bmatrix} = \begin{bmatrix} I_S e^{j(\omega_1 t-\varphi_1)} + I'_S e^{j[(1-2s)\omega_1 t-\varphi_1]} \\ I_S e^{-j(\omega_1 t-\varphi_1)} + I'_S e^{-j[(1-2s)\omega_1 t-\varphi_1]} \\ 0 \end{bmatrix} \tag{2}$$

where I_S and I'_S are the stator currents with the frequency of ω_1 and $(1-2s)\omega_1$, respectively; V_1, V_2, and V_0 are the positive sequence, negative sequence, and neutral components of the stator voltage expressed in the 120 system; φ_1 is the angle that I_S lags V_S; and φ_2 is the angle that I'_S lags V_S; ω_1 is the synchronous angular frequency. A ***bold*** letter indicates a phasor while a normal letter indicates its amplitude.

Total power delivered to the motor is

$$\begin{aligned} P_1 &= \mathrm{Re}\{\boldsymbol{V}_1 \boldsymbol{I}^*_1 + \boldsymbol{V}_2 \boldsymbol{I}^*_2\} \\ &= V_S I_S e^{j\varphi} + V_S I_S e^{-j\varphi} + V_S I'_S e^{j[2s\omega_1 t+\varphi_2]} \\ &\quad + V_S I'_S e^{-j[2s\omega_1 t+\varphi_2]} \\ &= 2[V_S I_S \cos\varphi_1 + V_S I'_S \cos(2s\omega_1 t+\varphi_2)]. \end{aligned} \tag{3}$$

The total developed average torque of the synchronous motor can be derived, by subtracting the copper losses from the total power, and then divided by the synchronous speed

$$T = \frac{2p}{\omega_1}\mathrm{Re}\left\{\left(V_1 - \boldsymbol{I}_S r_1 - \boldsymbol{I}'_S \frac{r_1}{1-2s}\right)\cdot I^*_1\right\} \tag{4}$$

where p is the total number of poles.

During the starting of synchronous motors, the two components of stator current have different frequencies, only the constant terms constitute the average torque and the other terms give the pulsating torque. The average torque is

$$T_a = \frac{2p}{\omega_1}\left(V_S I_S \cos\varphi_1 - I^2_S r_1 - I'^2_S \frac{r_1}{1-2s}\right). \tag{5}$$

The pulsating torque is

$$\begin{aligned} T_p &= \frac{2p}{\omega_1}\mathrm{Re}\left\{V_S I'_S e^{j(2s\omega_1 t+\varphi_2)}\right. \\ &\qquad -I_S I'_S \frac{r_1}{1-2s} e^{-j(2s\omega_1 t-\varphi_1+\varphi_2)} \\ &\qquad \left. -I_S I'_S r_1 e^{j(2s\omega_1 t-\varphi_1+\varphi_2)}\right\} \\ &= \frac{2p}{\omega_1}\left\{V_S I'_S \cos(2s\omega_1 t+\varphi_2)\right. \\ &\qquad -I_S I'_S \frac{r_1}{1-2s}\cos(2s\omega_1 t-\varphi_1+\varphi_2) \\ &\qquad \left. -I_S I'_S r_1 \cos(2s\omega_1 t-\varphi_1+\varphi_2)\right\}. \end{aligned} \tag{6}$$

By using (5) and (6), the average torque and the pulsating torque can be calculated for given I_S, I'_S, and V_S and parameters of the motor. The calculation of stator currents I_S, I'_S will be further discussed.

D. Stator Currents

During the starting, the stator voltage V_S rotates at the synchronous speed, while the rotor d–q frame rotates at the rotor speed. Therefore, the angle between the stator voltage and the rotor q axis is $\{\omega_1-(1-s)\omega_1\} = \{s\omega_1+\theta\}$, where θ is the final angle between stator voltage and rotor q axis at synchronous speed. $V_d = jV_S\sin(s\omega_1 t+\theta)$ and $V_q = V_S\cos(s\omega_1 t+\theta)$. It is clear that both V_d and V_q varies between $-V_S$ and V_S. When rotor d axis aligns up with the stator voltage, $V_q = V_S$; when q axis aligns up with the stator voltage, $V_d = V_S$. The stator current can be solved by averaging the current at these two particular positions.

As analyzed above, the stator current has two components during starting. Using the equivalent circuit given in Fig. 1, let

$$z_d = r_1 + jx_1 + \frac{1}{\frac{1}{jx_{ad}} + \frac{1}{\frac{r_{2d}}{s}+jx_{2d}} + \frac{1}{\frac{r_f}{s}+jx_f}} \tag{7}$$

$$z_q = r_1 + jx_1 + \frac{1}{\frac{1}{jx_{aq}} + \frac{1}{\frac{r_{2q}}{s}+jx_{2q}}} \tag{8}$$

$$z'_d = \frac{r_1}{1-2s} + jx_1 + \frac{1}{\frac{1}{jx_{ad}} + \frac{1}{\frac{r_{2d}}{s}+jx_{2d}} + \frac{1}{\frac{r_f}{s}+jx_f}} \tag{9}$$

$$z'_q = \frac{r_1}{1-2s} + jx_1 + \frac{1}{\frac{1}{jx_{aq}} + \frac{1}{\frac{r_{2q}}{s}+jx_{2q}}}. \tag{10}$$

When the rotor q axis aligns up with the stator voltage, $V_d = V_1$, therefore

$$\boldsymbol{V}_S = \boldsymbol{I}_S z_d + \boldsymbol{I}'_S z'_d. \tag{11}$$

When the rotor d axis aligns up with the stator voltage, $V_q = V_1$, therefore

$$\boldsymbol{V}_S = \boldsymbol{I}_S z_q - \boldsymbol{I}'_S z'_q. \tag{12}$$

Solving for $\boldsymbol{I}_1$ and $\boldsymbol{I}_2$ from (11) and (12), the synchronous component and the $(1-2s)$ component of the stator current can be derived

$$\boldsymbol{I}_S = \boldsymbol{V}_S \frac{z'_q + z'_d}{z_d z'_q + z_q z'_d} = I_S \angle -\varphi_1 \tag{13}$$

and

$$\boldsymbol{I}'_S = \boldsymbol{V}_S \frac{z_q - z_d}{z_d z'_q + z_q z'_d} = \boldsymbol{V}_S \frac{z'_q - z'_d}{z_d z'_q + z_q z'_d} = I'_S \angle -\varphi_2. \tag{14}$$

The kinematic equations of the system can be written as

$$J\frac{d\omega}{dt} = T_a + T_p - T_0 - T_L. \tag{15}$$

Therefore, the starting performance can be simulated using the analytical model developed above. Fig. 2 shows the simulated starting torque-speed curve of the pump-storage motor.

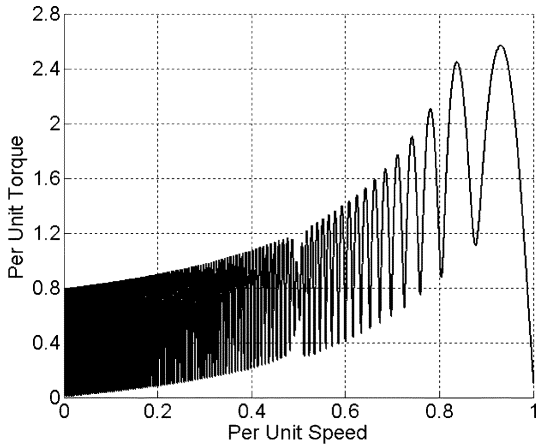

Fig. 2. Simulated torque speed curve of the pump-storage motor.

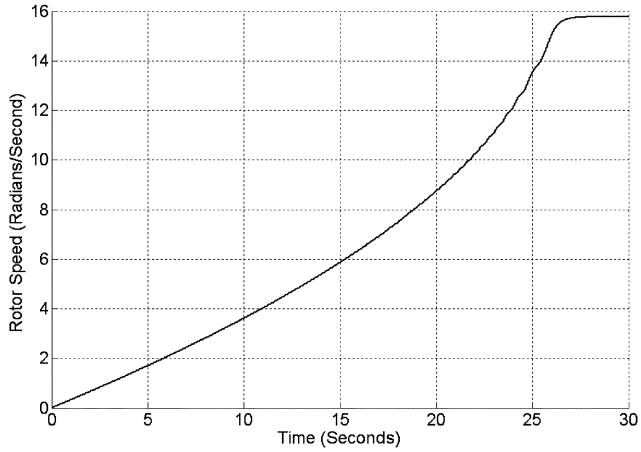

Fig. 3. Simulated acceleration of the pump-storage motor. The acceleration time to reach synchronous speed is approximately 27 s for unwatered start.

Fig. 3 shows the motor speed as a function of time for the unwatered case. It can be seen from Fig. 3 that the acceleration time for the unwatered case is approximately 27 s.

III. Finite-Element Modeling

The equivalent circuit model can be used to simulate the starting process, but it relies on other methods such as FEA to provide circuit parameters for different slips. It can only provide an average damper current, not the distribution in each rotor bar, nor the temperature of the damper bars. Therefore, time-stepping FEA is a powerful tool to simulate the damper bar current distributions, electromagnetic torque, acceleration, and temperatures. It can also be used to provide equivalent circuit parameters for other uses and perform in-depth analysis of the starting performance of large salient-pole synchronous motors. FEA was used in this study to understand the damper bar current and temperature distribution.

The mathematical formulations and the development of the software package for design applications have been described in [1]. Only the features of the modeling for its application to the pumped storage units' starting calculation are given in this paper.

The stator of each unit has 396 slots and the rotor has 48 poles. Each of the rotor poles has six damper bars. The damper bars are connected through end ring. Since the number of stator slots per pole per phase is $2\frac{3}{4}$, the field repeats every four poles. Therefore, a four-pole model is required for modeling the winding pattern. The stator coils have four turns/coil and the individual turns of the stator coils are modeled in the FEA model. The field coils are strip-wound and have 38 turns/pole. Each of the field winding turns is also modeled.

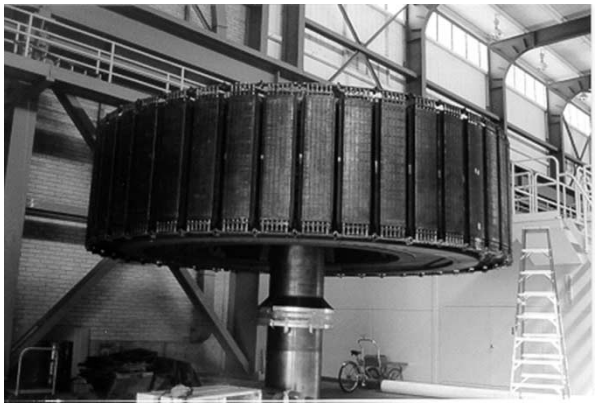

Fig. 4. Rotor of one of the pumped storage units.

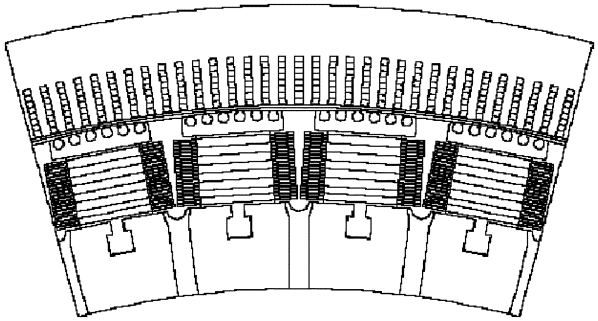

Fig. 5. Finite-element model outline.

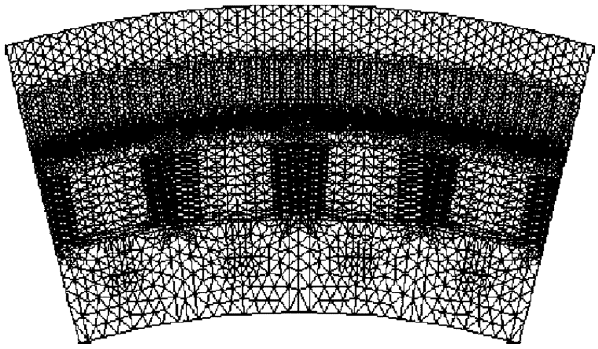

Fig. 6. Detailed mesh for the finite-element analysis.

Fig. 4 shows the rotor of one of the units on the shaft. Alternative rotor designs were considered to study the effects of design changes on the starting performance of the pump motors. Fig. 5 shows the FEA model outline spanning four rotor poles for the existing rotor design. Alternate damper winding designs were considered for the study to minimize the variation of thermal expansion among the damper bars. Fig. 6 shows the discretization of the model of Fig. 5 in triangular first-order finite elements for two-dimensional nonlinear eddy-current field problem.

The three-dimensional effects were included in the coupled field-circuit formulation by using end-leakage reactances and the end winding resistances as external circuit parameters. The model of Fig. 6 has 29 574 elements and 15 279 nodes. The selection of mesh density is a tradeoff between the desired accuracy of the results and the computer CPU times. An automatic mesh generator was developed by the first author and his associates to generate the FEA models depending on the application. Some trial and error are often required to determine the appropriate mesh density to achieve an accurate solution in a reasonable time frame. In addition, to compute the eddy-current distribution in damper bars accurately during starting, very fine mesh in the damper bars is required.

Rotor motion was modeled by connecting separate FEA models for the stator and the rotor along a sliding surface in the air gap [1]. The two models are connected electromagnetically by periodic and antiperiodic boundary conditions between the magnetic vector potential of the coinciding nodes along the two sides of the sliding surface [8].

At each time step after the start of the simulation, the new rotor position is determined by the calculated speed of the rotor. In this method of simulation, rotor motion is restricted to be in increments of the element size on the sliding surface. The number of elements on the sliding surface is large enough to model rotor speed accurately during acceleration.

The main advantage of the sliding surface method for simulation of rotor motion is that no new mesh generation is required at different rotor positions, which keeps the mesh topology constant throughout the simulation. The discretization error in finite-element mesh remains constant, thereby improving the accuracy of the time-stepping simulations significantly.

The rotor speed at each time step is obtained from the solution of the kinematic equation of the shaft system. For the watered start case, the load torque varies with speed. For the simulation of the acceleration of the rotor for watered starting, the actual load torque-speed curve was replaced by a staircase over a large number of speed intervals. This requires the analyst to stop and restart the simulation every time a certain speed is reached. At every time step, the electromagnetic air gap torque is calculated from the electromagnetic field solution by using the Maxwell stress tensor method. The rotor speed and position at each time step is obtained by using one-step explicit Euler difference scheme for the kinematic equation. The kinematic system is solved decoupled from the field-circuit system, which does not pose any risk of instability or loss of accuracy because of the large mechanical time constants of the motor/generator units.

IV. Simulation Results

The simulated acceleration curve using time stepping FEA for the unwatered starting of the pump-storage motor is shown in Fig. 7, which indicates a 28.2 s acceleration time to synchronous speed. The field distribution at start, at half speed, and at near synchronous speed are shown in Figs. 8–10, respectively. It can be seen from Figs. 8–10 that the flux penetrates gradually in the rotor pole body during acceleration to synchronous speed due to the reaction of the damper bar currents, which remain practically the same during the acceleration. The damper bar currents in the trailing and leading bars of the right pole during acceleration are shown in Figs. 11 and 12, respectively, for watered starts. It can

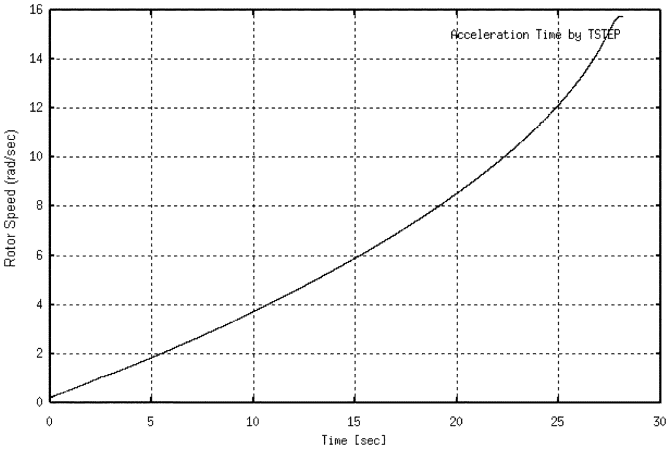

Fig. 7. Calculated acceleration of the pump-storage motor for unwatered starts. The acceleration time to synchronous speed is 28.2 s.

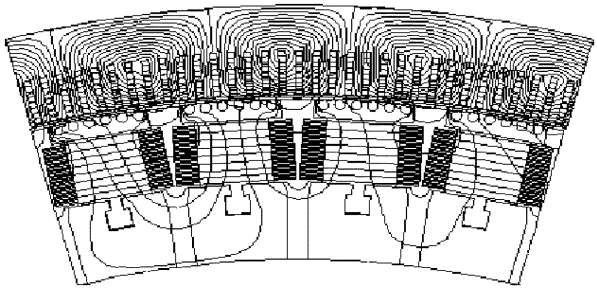

Fig. 8. Field distribution during initial start.

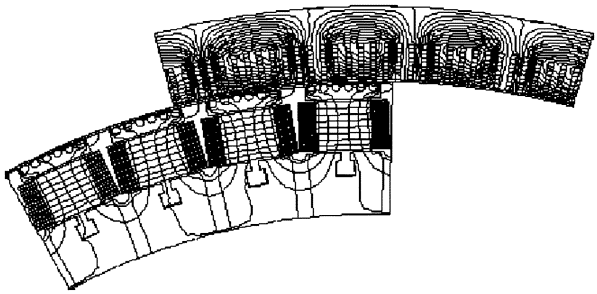

Fig. 9. Field distribution at about half synchronous speed.

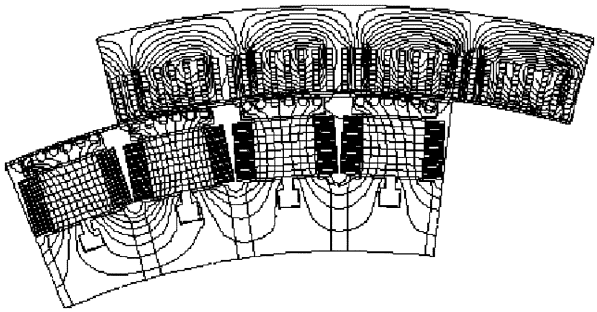

Fig. 10. Field distribution at near synchronous speed.

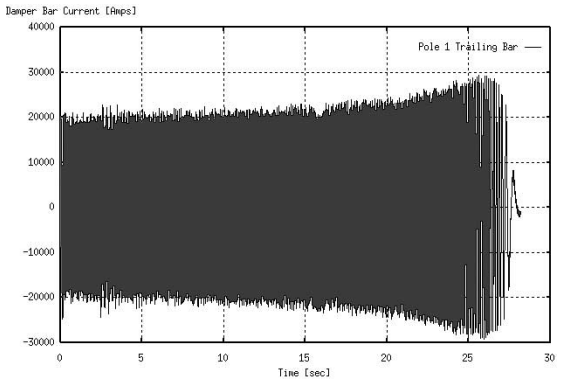

Fig. 11. Trailing damper bar current in pole 1 during acceleration.

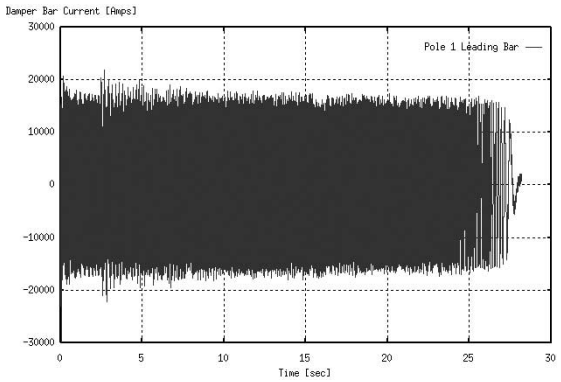

Fig. 12. Leading damper bar current in pole 1 during acceleration.

be seen from Figs. 11 and 12 that the trailing bar carries higher current than the leading bar. To calculate the thermal expansion of the damper bars, an effective value of the damper bar current is calculated by integrating the current squared over the acceleration time and taking the square root. The power loss in the bar equals the effective average current squared times the bar resistance.

Table II shows the currents in the damper bars for all bars in four poles of the FEA model for the unwatered case. Poles and bars are counted from right to left. The damper bar 1 is located at the trailing edge and the bar 6 is at the leading edge of the poles. It can be seen from Table II that the trailing edge bar carries higher current than the leading edge bar. The nonuniform distribution of currents in the bar will give rise to nonuniform thermal expansion, which has to be accommodated in the design of the damper winding and the shorting end rings.

The simulation of watered starts is performed by dividing the load torque-speed characteristic into a number of segments of speed intervals. Over each speed interval, an average value of load torque is used to calculate the acceleration and speed as functions of time. Table III shows the results of simulation for the effective damper bar currents for the watered start. It can be seen from Table III that the bar currents are again unevenly distributed, with the trailing edge bar carrying higher current than the leading edge bar.

It can also be seen from Tables II and III that the bar currents are not evenly distributed for damper bars under different poles. The difference in the damper bar current will develop uneven temperature rise in damper bars and end rings; therefore,

TABLE II
INTEGRATED DAMPER BAR CURRENTS FOR UNWATERED START

	POLE 1	POLE 2	POLE 3	POLE 4	AVG
BAR 1	14683.7	12483.7	12289.1	12510	12991.6
BAR 2	9714.5	9642.0	9637.1	9645.4	9659.7
BAR 3	9380.2	9383.6	9379.7	9387.9	9382.8
BAR 4	9181.4	9204.8	9191.7	9189.9	9191.9
BAR 5	8924.7	8995.5	8937.4	8573.3	8857.7
BAR 6	10789.1	11132.0	10788.7	8144.2	10213.5

TABLE III
INTEGRATED DAMPER BAR CURRENTS FOR WATERED START

	POLE1	POLE2	POLE3	POLE4	AVG
BAR 1	14932.1	12382.6	12175.2	12383.8	12968.4
BAR 2	9367.4	9298.5	9295.1	9265.0	9306.5
BAR 3	9064.4	9095.3	9136.0	9071.2	9091.7
BAR 4	9016.1	9076.7	9003.5	9009.7	9026.5
BAR 5	8913.9	8971.5	8893.9	8523.3	8825.7
BAR 6	10706.8	11099.9	10788.7	7760.3	10088.9

TABLE IV
CALCULATED AND MEASURED EFFECTIVE DAMPER BAR TEMPERATURE FOR WATERED START

BAR	BAR1	BAR2	BAR3	BAR4	BAR5	BAR6
CALCULATED	161.5	83.2	79.4	78.3	74.8	97.8
MEASURED	132.2	108.5	96.8	83.0	76.9	96.8

nonuniform expansion will occur. This should be taken into consideration during the design of these motors.

The temperature rise of the damper bars are calculated by

$$\Delta T = \frac{P_C}{C_p m}\Delta t \tag{16}$$

where C_p is the specific heat of the damper bars, m is the weight of the bar, Δt is the elapsed time, and P_C is the total loss in the each damper bar, which can be expressed as

$$P_C = (I_{\text{bar}})^2 R_{\text{bar}} \tag{17}$$

where I_{bar} and R_{bar} are the effective damper current and resistance, respectively.

The calculated effective bar temperature rise is shown in Table IV. For comparison purposes, the measured temperature rise during the acceleration time is also shown in the same table.

V. SITE TEST

Special site tests were performed to measure the acceleration time and determine the temperatures of the damper bars during starting. The damper bars on one rotor pole on one of the units were instrumented with thermistors.

The thermistors were inserted into the holes in the damper bars so that the elements of the thermistors were seated at the bottom of the hole and secured. The outputs of the thermistors were connected to a data acquisition system to store data during

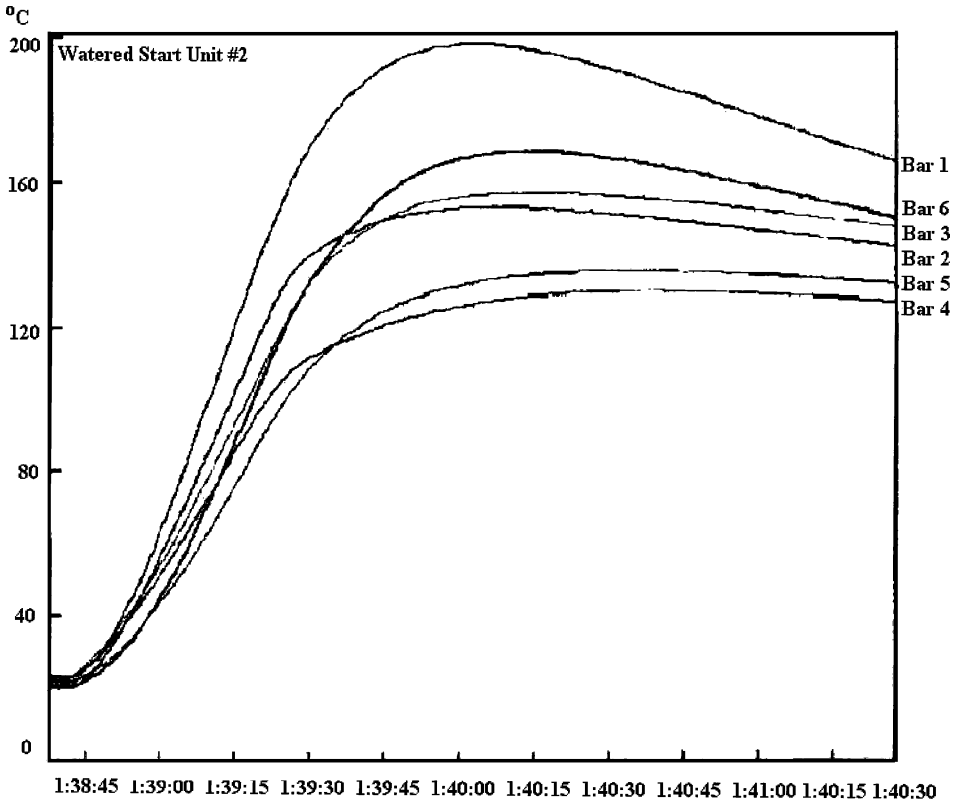

Fig. 13. Tested bar temperature of the pump-storage motor.

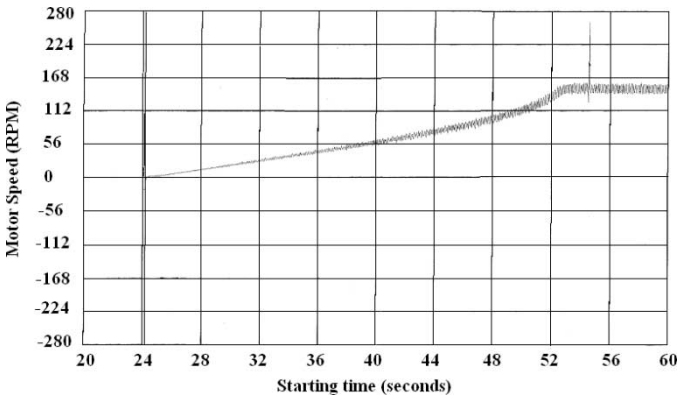

Fig. 14. Acceleration of the pump-storage motor tested on site. The measured acceleration time is 28.5 s.

startups at various conditions. Fig. 13 shows the measured bar temperature for the watered start of the pump-storage motor. The measured effective bar temperature rise during the acceleration time is also shown in Table IV. It can be seen from Table IV that the temperature calculations follows the trend of measurement for the practical design purposes. It also shows that bar 1 temperature rise is much higher than any other bar as predicted in the simulations. The accurate temperature rise calculation requires complex computational fluid dynamics (CFD) models, which were not warranted for these studies.

The acceleration times were recorded by using a speed monitor during startups for both watered and unwatered cases. The tested acceleration of the pump-storage motor for the unwatered case is shown in Fig. 14. The measured acceleration time of both watered and unwatered cases are shown in Table V. It can be

TABLE V
ACCELERATION TIMES OF THE STUDIED PUMP-STORAGE SYNCHRONOUS MOTOR (SECONDS)

	FEA MODEL	ANALYTICALMODEL	MEASUREMENT
UNWATERED START	28.2	27.0	28.5
WATERED START	39.3	38.0	42.9

seen from Table V that both analytical model and FEA model give good estimation of the acceleration time. The most possible cause for the discrepancy between the calculated and test acceleration time for the watered case is the representation of load torque over the entire speed range from start to synchronous by segmenting into several speed intervals. By increasing the speed intervals, the discrepancy with test results could be reduced at the expense of increased simulation time. Since the purpose of the study is to obtain relative differences in the performance by design variations, additional attempts to reduce the discrepancy between the calculated and test results were not felt warranted. On the other hand, there is a stick friction just at the starting of the system. Therefore, the rotation of the motor begins only when the motor torque is larger than the stick friction torque. The viscous friction is usually larger at low speeds than at high speeds. This force was not represented in the mathematical model, which may also have contributed to the discrepancy with test results.

VI. ALTERNATE ROTOR DESIGN STUDIES

The consistence between the simulation and site tests laid ground for further studies. Following completion of the simu-

lation of the existing damper bar designs with respect to both unwatered and watered start, a number of alternative designs were simulated with the goal of reducing the differences in currents among the damper bars during the starting sequences. If the currents in the six damper bars could be made nearly equal, the design of the flexible connections between the damper bars and the shorting ring segments becomes less complicated.

Alternative rotor designs were simulated to study the effects of design changes on the starting performance of the pump storage units. The alternatives were studied to minimize the variation of thermal expansions in the damper bars. The following alternative designs were initially proposed to be studied:

- Replace brass damper bars by copper bars. The units were originally designed and built with naval brass damper bars with resistivity of 3.8 per unit of copper. Higher resistivity damper bars provide higher starting torque at the expense of pull-in torque. Lower resistivity bars increase pull-in torque at the expense of starting torque. Since there is no particular starting torque requirement for the pump motor units, the change of material to copper was studied to verify the current and temperature distribution in the bars to improve the starting performance. The main criterion used is that the damper bar temperature distribution is within the allowable limits tested at the site. The bar material and diameter are also selected to keep stress due to centrifugal force within permissible limits.
- Replace six bars/pole with five bars/pole. The number of damper bars is selected by considering the pole enclosure and the number of stator slots per pole. For these units, other possible variations of the number of bars are five or seven damper bars. The seven bar design was not considered for mechanical reasons.
- Mix brass and copper bars by replacing only the outermost bars by copper bars was also considered. This option was not studied because of past experience of unfavorable differential expansion between bars for motors for other pumped storage units.

Therefore, the alternative designs considered for simulation are as follows:

1) Starting with an external reactor in the stator winding. Some reactors were purchased with the original units for such starts, but were never used for lacking of data.
2) Changing the existing naval brass bars with copper bars.
3) Changing the number of damper bars per pole from six to five copper bars.

The alternative study was focused on both watered and unwatered start. The data in Tables VI–VIII are shown for the watered start. Table VI shows the simulated damper bar currents for the reactor start. It can be seen from Table VI that the reactor-start decreases the damper bar currents and distributes them more uniformly among the bars. Table VII shows the simulated damper bar current for alternative 2: change the damper bars from brass to copper. The current distribution in the bars did not show any improvement over brass bars. Table VIII shows the calculated damper bar currents for alternatives 3: change to damper bars from six to five. Again, the five copper bars did not show any improvement in the current distribution. Table IX further compares the acceleration time for all three different alternatives with the original design. It can be seen from Table IX that the original design is better than any of the proposed alternative designs in terms of acceleration time. In the case of reactor start, the acceleration time is more than doubled.

TABLE VI
INTEGRATED DAMPER BAR CURRENTS FOR REACTOR START

	POLE1	POLE2	POLE3	POLE4	AVG
BAR 1	12069.4	10043.2	9885.8	10060.2	10514.7
BAR 2	7886.8	7788.8	7778.2	7797.1	7812.7
BAR 3	7525.4	7523.7	7527.7	7534.5	7527.8
BAR 4	7360.9	7375.4	7363.2	7364.3	7366.0
BAR 5	7147.9	7211.9	7159.9	6821.7	7085.3
BAR 6	8583.7	8868.6	8615.7	6096.9	8041.2

TABLE VII
INTEGRATED DAMPER BAR CURRENTS FOR SIX COPPER BARS

	POLE1	POLE2	POLE3	POLE4	AVG
BAR 1	13581.4	12706.2	12629.8	12616.6	12883.5
BAR 2	9895.4	9868.4	9825.7	9830.0	9854.9
BAR 3	9771.1	9768.1	9765.5	9784.0	9772.2
BAR 4	9687.2	9697.7	9692.8	9702.8	9695.1
BAR 5	9396.3	9394.4	9351.5	9296.3	9359.6
BAR 6	11375.8	11592.3	11408.4	10158.2	11133.7

TABLE VIII
INTEGRATED DAMPER BAR CURRENTS FOR FIVE DAMPER BARS

	POLE1	POLE2	POLE3	POLE4	AVG
BAR 1	14140.1	13677.6	13633.4	13686.8	13784.5
BAR 2	9915.5	9893.9	9886.2	9896.8	9898.1
BAR 3	9701.0	9697.1	9700.1	9709.1	9701.8
BAR 4	9491.8	9505.5	9495.0	9470.5	9490.7
BAR 5	12448.7	12534.9	12465.0	11748.9	12299.4

TABLE IX
ACCELERATION TIME OF THE PUMP-STORAGE SYNCHRONOUS MOTOR: WATERED START (SECONDS)

	SIMULATED ACCELERATION TIME
THE EXISTING PUMP STORAGE MOTOR	39.3
WITH REACTOR START	87.1
CHANGE TO COPPER DAMPER BARS	70.6
CHANGE TO FIVE DAMPER BARS	68.6

Based on these simulation studies, it was concluded that the best choice was to keep the original damper bar designs and concentrate on the redesign of the flexible connectors for the desired number of additional starting cycles. The FEA and analytical model provided means of studying these alternatives without having to make the expensive implementation of the design alternatives.

VII. CONCLUSION

The equivalent circuit model provides an acceptable yet simple approach for the design and simulation of large salient-pole synchronous motors. Time-stepping FEA provides

a powerful tool for the simulation of both steady-state and transient performance of large synchronous machines to calculate detailed distribution of fields and currents. Both methods, verified by experiments, provide an analytical tool to perform engineering studies for large salient-pole synchronous motors. The transient starting performance for a pumped storage motor/generator unit was simulated to study alternative designs and their effects on the starting performance of the pump motor to improve the reliability of the starting system. The simulation results were verified by on site tests. The results of thermal and mechanical analysis using the calculated damper bar currents were also verified using the site test results of damper bar temperatures.

Based on the simulation results, the flexible connectors have been designed to ensure the accommodation of the differential thermal expansions among the damper bars for the desired additional starting cycles.

ACKNOWLEDGMENT

The authors would like to acknowledge the technical discussions and contributions by D. Cole, D. McLaren, and R. Horton during the execution of these studies, which constituted a part of the engineering study performed for the customer.

REFERENCES

[1] H. Karmaker, "Practical design applications of time-stepping finite element analysis to salient-pole synchronous machines," in *Proc. IEEE PES Winter Meeting*, 2000.

[2] K. Weeber, "Determination of dynamic parameters of large hydro-generators by finite-element simulation of three-phase sudden short circuits," in *Proc. IEMDC*, 1997.

[3] S. Nabeta, A. Foggia, J. Coulomb, and G. Reyne, "A time-stepped finite-element simulation of a symmetrical short-circuit in a synchronous machine," *IEEE Trans. Magn.*, vol. 30, pp. 3683–3683, Sept. 1994.

[4] A. Kladas and A. Razek, "Eddy currents modeling in synchronous machines during starting accounting for the nature of damper end connections," *IEEE Trans. Magn.*, vol. 24, pp. 186–186, 1988.

[5] Y. Xiao, G. Slemon, and M. Iravani, "Implementation of an equivalent circuit approach to the analysis of synchronous machines," *IEEE Trans. Energy Conversion*, vol. 9, pp. 717–717, Dec. 1994.

[6] J. H. Dymond, B. Mistry, and R. Ong, "Acceleration tests to determine salient pole synchronous motor inrush currents and torques," *IEEE Ind. Applicat. Mag.*, July/Aug. 2002.

[7] J. O. Ojo, V. Ostovic, T. A. Lipo, and J. C. White, "Measurement and computation of starting torque pulsations of salient pole synchronous motors," *IEEE Trans. Energy Conversion*, vol. 5, pp. 176–182, Mar. 1990.

[8] I. Tsukerman, J. Lavers, A. Konrad, K. Weeber, and H. Karmaker, "Finite element analysis of static and time-dependent fields and forces in a synchronous motor," in *Proc. ICEM*, 1994.

Haran Karmaker (S'70–M'74–SM'82) received the B.Sc. Eng. degree from Bangladesh University of Engineering and Technology, Dhaka, Bangladesh, in 1967, and the M.A.Sc. and Ph.D. degrees from the University of Toronto, Toronto, ON, Canada, in 1971 and 1974, respectively, all in electrical engineering.

He joined the Engineering Laboratory of General Electric Canada, Peterborough, ON, as a Research Engineer in 1975. Since 1981, he has been the Technical Leader of the Electromagnetics Team. He has led successful completion of many large collaborative research projects with Canadian and U.S. universities funded by GE, Canadian, and U.S. Governments. In 1999, his team won the GE Industrial Systems Six Sigma Modeling Contest on Electrical Losses in Synchronous Machines. He has presented and published over 40 technical papers in IEEE, IEE, ICEM and other international journals. He is a co-author of the 2004 edition of *Handbook of Electric Motors* (New York: Marcel Dekker). His primary research activities include simulation and modeling of large rotating electrical machines, power electronic drives, and experimental studies for machine parameters, fields, and losses. He has served IEEE Canada as Chair of Peterborough Section, Central Canada Council, Professional Development, and Educational Activities Committees. He is a member of the IEC Technical Committees on Magnetic Steels and Rotating Machinery and the NEMA Rotating Electrical Machinery Committee. He has contributed to the development of IEEE, IEC and NEMA standards. He is the current Chair of the Working Group on Revision of IEEE Standard 115 "Test Procedures for Synchronous Machines."

Dr. Karmaker is a registered Professional Engineer in Ontario.

Chunting Mi (S'00–A'01–M'01–SM'03) received the B.S.E.E. and M.S.E.E. degrees from Northwestern Polytechnical University, Xi'an, China, and the Ph.D. degree from the University of Toronto, Toronto, ON, Canada, all in electrical engineering.

He is an Assistant Professor at the University of Michigan, Dearborn, with teaching responsibilities in the area of power electronics, electric vehicles, electric machines and electric drives. He joined General Electric Canada Inc. as an Electrical Engineer in 2000, responsible for designing and developing large electric motors and generators. He started his career in 1988 at the Rare-Earth Permanent Magnet Machine Institute of Northwestern Polytechnical University. He joined Xi'an Petroleum Institute as an Associate Professor and Associate Chair of the Department of Automation in 1994. He was a Visiting Scientist at the University of Toronto from 1996 to 1997. He has recently developed a Power Electronics and Electrical Drives Laboratory at the University of Michigan, Dearborn. His research interests are electric drives, power electronics, induction motors, brushless motors, and permanent-magnet synchronous machines; renewable energy systems; electrical and hybrid vehicle powertrain design and modeling. He is the Chair of the Power Electronics and Industrial Electronics Chapter of the IEEE Southeast Michigan Section.